XFEL.EU TR-2018-001

TECHNICAL REPORT

Performance of the SASE3 monochromator equipped with a provisional short grating. Variable line spacing grating specifications

May 2018

N. Gerasimova

for the X-Ray Optics and Beam Transport group (WP73)

at the European XFEL

European X-Ray Free-Electron Laser Facility GmbH

Holzkoppel 4

22869 Schenefeld

Germany

Abstract

The planned gratings for the soft X-ray monochromator at the SASE3 beamline demand extremely high production capabilities, which currently have not been achieved. In this report, the detailed specifications on the variable line spacing parameters of the gratings are set and the expected performance of a short provisional grating is presented.

Contents

Preface

The soft X-ray beamline SASE3 is equipped with a grating monochromator [1]. To allow diffraction-limited beam transport, the demands on X-ray optics are extremely high, sometimes beyond current production capabilities. The reflective optics must be up to 1 m long in order to accept full beam (ideally > 6 σ of Gaussian beam profile, > 4 σ as a reasonable conservative condition), and the slope errors should be minimized. These demands hold for the gratings of the soft X-ray monochromator, and the 500 mm long gratings have been specified. However, to date, the capability to produce 500 mm long gratings of quality is still missing. One of the limiting parameters is the accuracy of variable line spacing (vls) parameters, which govern the imaging properties of the grating. Deterioration of the imaging properties reduces resolving power and shifts the performance of the monochromator away from the Fourier limit, the important parameter for ultrafast scientific applications beamline designed for. The aberrations induced by miscut vls parameters increase with the length of the grating. The mechanical ruling could result in the required vls accuracy; however, a ruling of 500 mm long grating is still not available. On the other hand, holographic technology allows the production of long grating but misses vls accuracy. The second disadvantage of holographic technology is the laminar groove profile, which results in lower efficiency and limits X-ray flux on the grating due to a lower damage threshold compared to blazed grating possible along with mechanical ruling.

As an interim solution, the short (120 mm long) provisional laminar grating has been manufactured holographically. A way to produce long grating according to the optical design of the beamline is still to be established.

In this report, the accuracy of variable line spacing parameters is specified for the long (500 mm) and provisional short (120 mm) grating, and the performance of the SASE3 beamline operational with provisional short grating is presented.

1 Methods

Details on the optical design of the SASE3 monochromator can be found in Ref. [1]. In short, the monochromator consists of a pre-mirror providing meridional focusing of the beam onto the exit slit and a plane vls grating. There are two pre-mirrors operational at a fixed angle of incidence: (i) the low energy (LE) pre-mirror, which operates at a grazing angle of 20 mrad, and covers the energy range of 250–1500 eV, and (ii) the high energy (HE) pre-mirror, which operates at a grazing angle of 9 mrad and covers the energy range of 1.5–3 keV. The grating has a central line density of 50 l/mm and operates at a fixed included angle of 40 mrad with an LE pre-mirror or 18 mrad with an HE pre-mirror.

In the present report, the variable line spacing parameters and aberrations induced by miscut vls parameters have been estimated analytically using the geometrical theory of diffraction grating [2]. The accuracy of vls parameters over the operational range of the SASE3 monochromator have been set in order to keep grating aberrations below the instrument response function (best possible resolution with optimal vls).

The performance of the beamline operational with long (500 mm) and short (120 mm) gratings has been evaluated analytically over the SASE3 operational range. Grating efficiencies have been calculated using “Reflec” code [3], which is part of the “Ray” package [4] developed at the Berliner Elektronenspeicherring-Gesellschaft für Synchrotronstrahlung (BESSY). Finally, the wavefront propagation simulations have been applied using the WaveProperGator (WPG) framework [5] to confirm the analytically estimated performance of the beamline.

To estimate the beam footprint on the optics, and the consequent geometrical cut, the beam divergence has been estimated according to Ref. [7], based on the expected SASE beam properties for the case of low, 20 pC, electron beam charge corresponding to the case of large divergence presented in Ref. [8]. The resulting shape of the footprint on the grating was used to

estimate the pulse elongation, and the corresponding beam profile after the grating was used to retrieve the ultimate monochromatic instrument response function in the exit slit plane (resolution) by the Fourier transform. To obtain a final instrument response, the ultimate response was convoluted with a function representing the reduction of resolution by the slope error on optics and, eventually, aberrations due to a miscut of the vls parameter.

2 Variable line spacing parameters

A plane grating with a constant ruling parameter operational in convergent beam (the case of the SASE3 monochromator) introduces aberrations and deteriorates imaging properties of the grating and thus reduces the monochromator resolution. Although the beamline is designed as a low-resolution one in order to maintain short pulses, it is important to stay as close as possible to the Fourier limit in order to optimize simultaneously temporal and energy resolution. Any deterioration of the energy resolution by the beam transport optics (aberrations) would shift the performance of the monochromator away from the Fourier limit. To avoid a loss in resolution induced by aberrations, variable line spacing is applied. On the other hand, wrongly set vls parameters induce aberrations on their own.

In this section, the optimal vls parameters and their tolerances are derived for the case of a long (500 mm) and the provisional short (120 mm) gratings.

2.1 Grating aberrations and variable line spacing

The groove density in case of variable groove spacing can be expressed as

$$n(w) = b0 + b1*w + b2*w^2 + b3*w^3 + .. \quad (1)$$

where *b0* is the central groove density; *b1*, *b2*, *b3*, .. are higher-order vls parameters; and *w* is the coordinate along the grating (in the present work direction along the grating is positive along the beam direction projected onto the grating).

According to the geometrical theory of the grating [2], the optical path function F(w) can be expressed using Taylor expansion:

$$F = r + r' + wF_{10} + w^2F_{20} + l^2F_{02} + w^3F_{30} + wl^2F_{12} + w^2l^2F_{22} + w^4F_{40} + .. \quad (2)$$

where *r* is the source-to-grating distance; *r'* is the grating-to-image distance; and *l* is the coordinate on the grating perpendicular to *w*.

For the case of a plane grating:

$$\sin\alpha + \sin\beta + \mathrm{m}\lambda b0 = 0 \tag{3}$$

$$F_{20} = \frac{\cos^2\alpha}{2r} + \frac{\cos^2\beta}{2r'} + \mathrm{m}\lambda\frac{b1}{2} \tag{4}$$

$$F_{30} = \frac{1}{2} * (\frac{\cos^2\alpha}{r} * \frac{\sin\alpha}{r} + (\frac{\cos^2\beta}{r'}) * \frac{\sin\beta}{r'}) + \mathrm{m}\lambda\frac{b2}{3} \tag{5}$$

$$F_{40} = \frac{1}{8} * (\frac{\cos^2\alpha * (4 * \sin^2\alpha - \cos^2\alpha)}{r^3} + \frac{\cos^2\beta * (4 * \sin^2\beta - \cos^2\beta)}{r'^3}) + \mathrm{m}\lambda\frac{b3}{4} \tag{6}$$

where *α* is the angle of incidence on the grating; *β* is the diffraction angle; *m* is the diffraction order; and *λ* is the wavelength.

To compensate for aberrations introduced by grating operational in non-collimated light, setting the $F_{ij} = 0$ condition will result in an optimal vls parameter. On the other hand, the aberrations in case of non-optimal vls parameters can be evaluated from the condition

$$\Delta = \frac{\partial F}{\partial w}\frac{r'}{\cos\beta}. \tag{7}$$

Thus, the aberrations due to a miscut of *b1* would be proportional to the first power of grating length, *b2* – to the second power of grating length, *b3* – to the third power of grating length, etc. This sets increasingly high demands on higher-order vls parameters with an increase of grating length.

2.2 Variable line spacing parameters and their tolerances for the SASE3 monochromator gratings

In the case of the SASE3 monochromator, plane grating operates in convergent light focused onto the exit slit: $r = -r'$; $r' = 99m$. The central groove density is $b0 = 50l/mm$. The optimal vls parameters are: $b1 = 1.01*10^{-3} l/mm^2$, $b2 = 1.53*10^{-8} l/mm^3$, and $b3 = 2.06*10^{-13} l/mm^4$. As shown below (Figs. 2–3), the optimal *b3* parameter is negligible and the optimal *b2* parameter is low compared to their tolerances; so both optimal *b3* and *b2* parameters can be set to 0.

To estimate tolerances on the vls parameters, the aberrations induced by each term in Eq. (2) have been set equal to half of the instrument response function in the focal plane calculated without taking into account grating aberrations (Sec. 3.3, Fig. 8). Such a condition would result in a resolution reduced by ~ 11% in the case of a Gaussian profile (i.e. a factor of ~ 1.12 increase in the width of the response function, the same decrease in the peak maximum of the response function). The illuminated part of the grating, namely full width at half maximum (FWHM) of the beam footprint, was taken into account to estimate aberrations due to the vls parameter.

The results of these analytical estimations over the SASE3 operation range is presented in Figs. 1–3. The increasing effect of the grating length on the vls parameters tolerances results from (i) the power dependence of aberrations on grating length discussed above and (ii) the narrower instrument response function (Figs. 8–9), i.e. higher possible resolving power, in the case of longer grating due to a higher number of illuminated grooves (Sec. 3.3 and 3.4). Looser tolerances with an increase of photon energy over the operation range of each pre-mirror result from (i) widening of the instrument response function (Figs. 8–9) and, (ii) in the case of long grating, from reduced aberration due to under-illumination of the grating with an increase of photon energy (beam footprint on the grating changes from < *2σ* to > *6σ,* increasing for each pre-mirror (Sec. 3.2, Fig. 7), in the case of long grating, and stays < *2σ* over the complete SASE3 energy range in the case of the short grating).

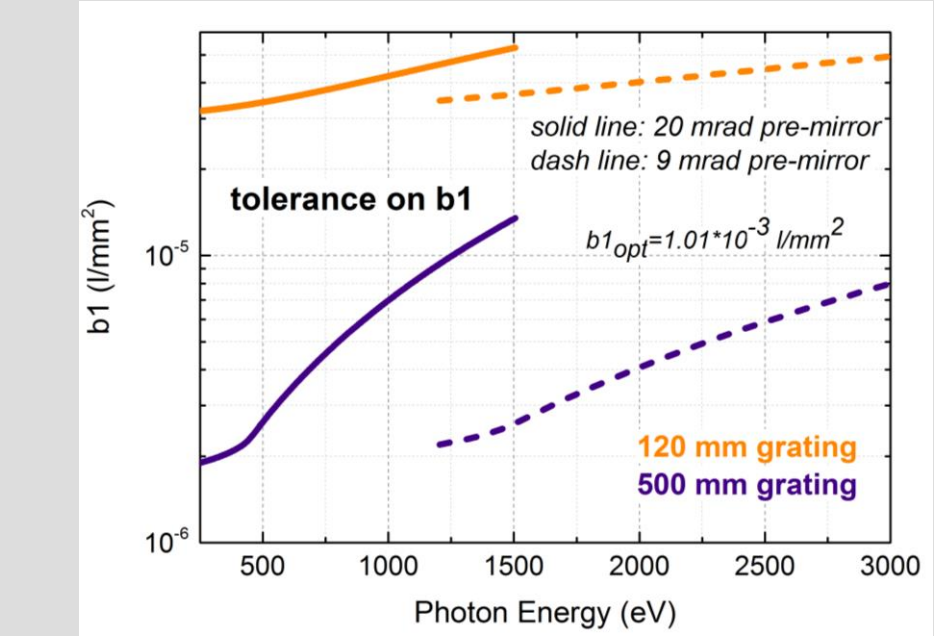

Figure 1: *Tolerances on the b1 parameter for provisional short (120 mm length, 200 nrad slope error) and design long (500 mm length,50 nrad slope error) gratings*

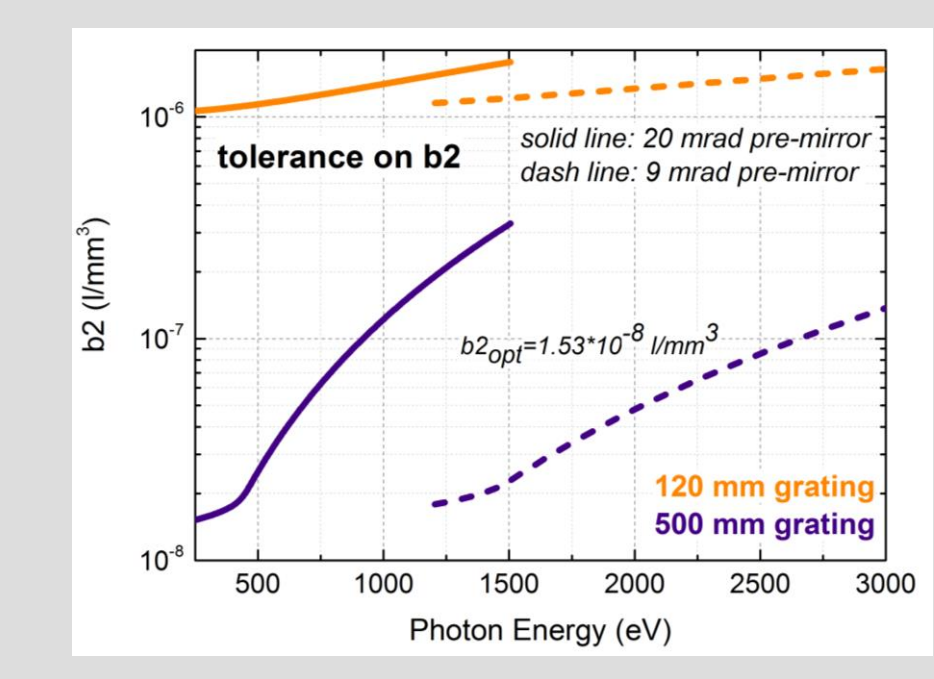

Figure 2: *Tolerances on the b2 parameter for provisional short (120 mm length, 200 nrad slope error) and design long (500 mm length,50 nrad slope error) gratings*

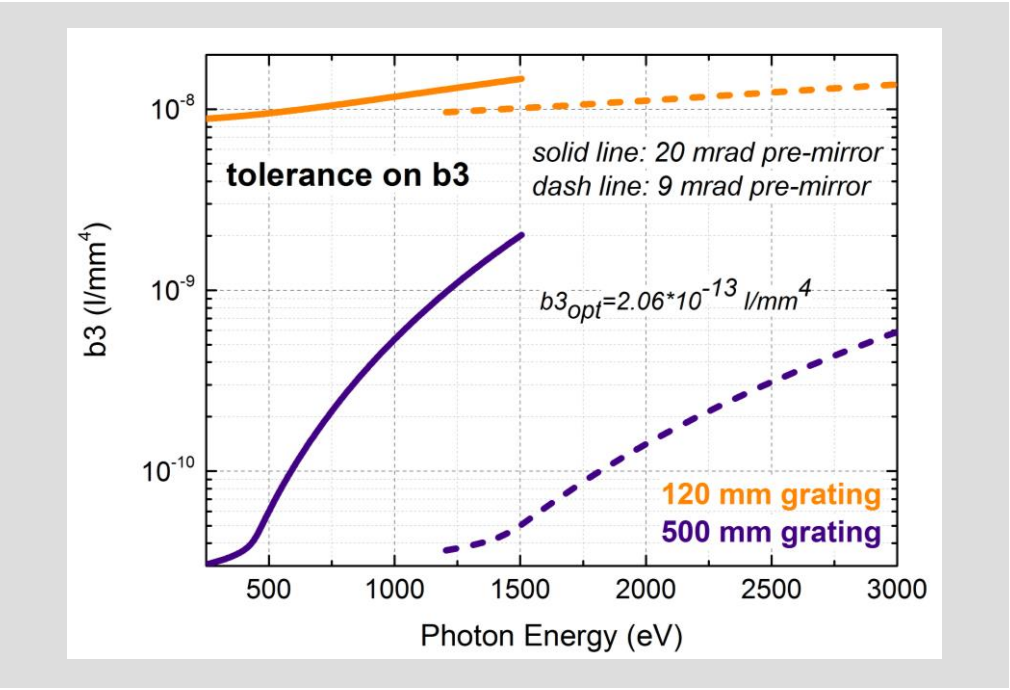

Figure 3: *Tolerances on the b3 parameter for provisional short (120 mm length, 200 nrad slope error) and design long (500 mm length,50 nrad slope error) gratings*

In order to verify the applicability of the analytical estimations, the wavefront propagation simulations have been applied for a set of photon energies. As an example, the instrument response functions for the case of more demanding long grating operated at 800 eV photon energy obtained using the WPG framework [5] are presented in Figs. 4–5. The surface errors used in the simulation have been chosen close to the specifications, namely 40 nrad rms slope error and 3.1 nm (3.4 nm) peak-to-valley height error on pre-mirror (grating). Note that the instrument response function without miscut vls parameter is already distorted by these surface errors. For the case presented in Figs. 4–5, the surface errors on the pre-mirror and the grating result in asymmetric instrument response (*b2 = 0 l/mm*^{3}, *b3 = 0 l/mm*^{4}: blue curves). Symmetric *b3*-related aberration just smears out the instrument response function when |*b3*| is above the optimal value (Fig. 5), and asymmetric *b2*-related aberration compensates the asymmetric slope error related profile for positive *b2*, thus shifting the optimal value of *b2* (Fig. 4). To quantitate distortion by miscut of vls parameters is not a straightforward task because of fringes in the instrument response profile. Here, the acceptable distortion is estimated as a decrease in the peak maximum of the instrument

response function by ~ 10 ÷ 15%. One can see a reasonably good agreement between analytical estimations and the wavefront propagation simulations; in the case of 800 eV, the analytically estimated tolerance on *b2,* $b2tol \approx 7*10^{-8} l/mm^3$ (Fig. 2), corresponds to similar distortion for $-3*10^{-8} l/mm^3 > b2 > -6*10^{-8} l/mm^3$ in the instrument response function in wavefront propagation simulations (Fig. 4). Similarly, the analytical estimation of tolerance on *b3*, $b3tol = 2.6*10^{-10} l/mm^4$ (Fig. 3), corresponds to $2*10^{-10} l/mm^4 < |b3| < 5*10^{-10} l/mm^4$ in wavefront propagation simulations (Fig. 4).

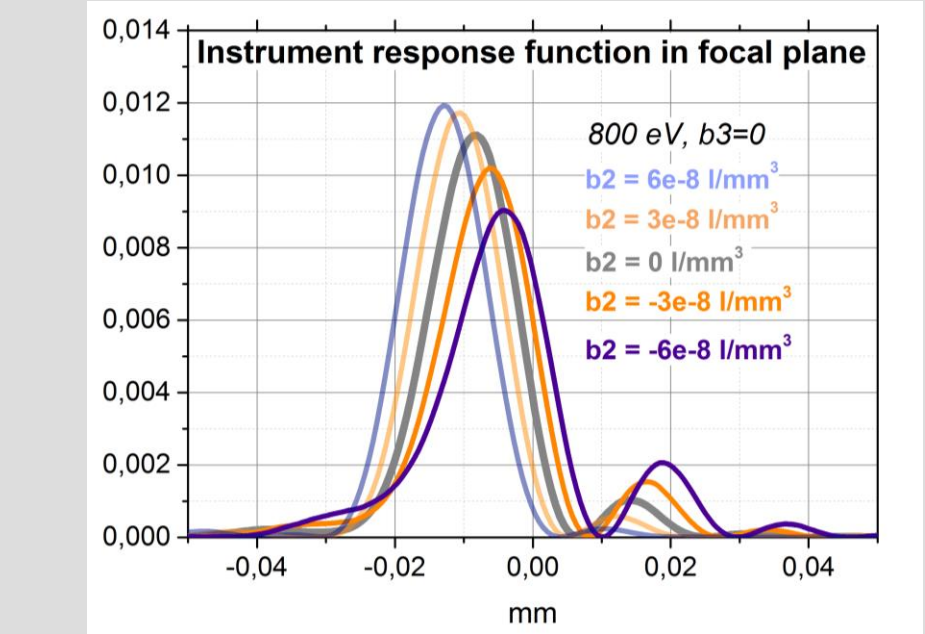

Figure 4: *Influence of the b2 parameter on the instrument response function in the focal plane for a 500 mm long grating at 800 eV; 40 nrad rms slope error, and 3.1 nm (3.4 nm) peak-to-valley height error on pre-mirror (grating)*

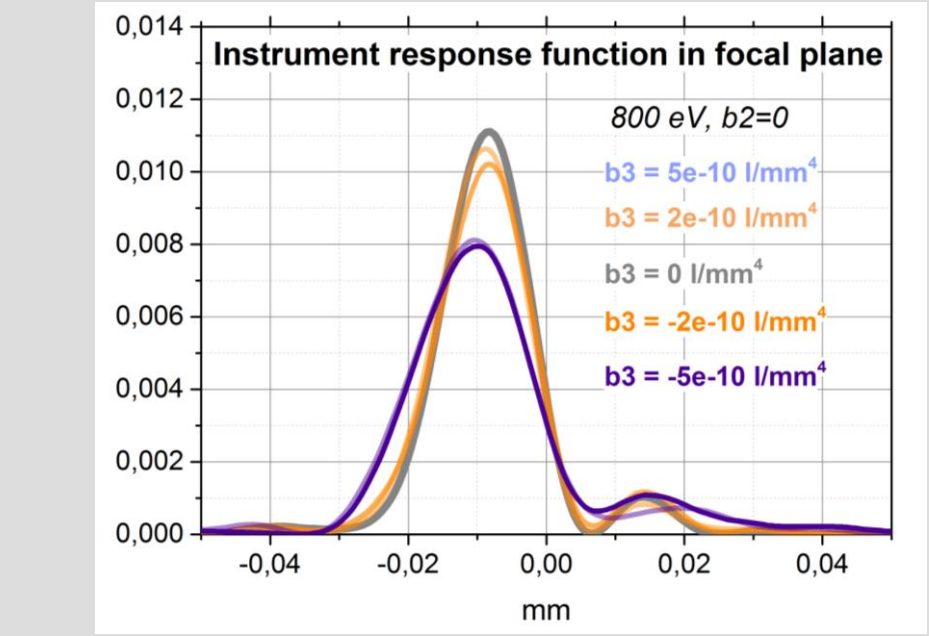

Figure 5: *Influence of the b3 parameter on the instrument response function in the focal plane for a 500 mm long grating at 800 eV; 40 nrad rms slope error, and 3.1 nm (3.4 nm) peak-to-valley height error on pre-mirror (grating)*

Although at low energies for each pre-mirror, the analytical estimations give slightly tighter tolerances ($b2tol \approx 2.5*10^{-8} l/mm^3$ at 500 eV and $b2tol \approx 1.5*10^{-8} l/mm^3$ at 250 eV) compared to wavefront propagation simulations giving similar distortion (for $b2 \approx -4*10^{-8} l/mm^3$ at 500 eV and $b2 \approx -3*10^{-8} l/mm^3$ at 250 eV). At high energies for each pre-mirror, the analytical estimations give slightly looser tolerances ($b2tol \approx 3*10^{-7} l/mm^3$ at 1500 eV for LE pre-mirror) compared to wavefront propagation simulations giving similar distortion at ($b2 \approx -1*10^{-7} l/mm^3$).

In summary, taking into account both analytical estimations and wavefront propagation results, one can set **tolerances on vls parameters in the case of a 500 mm long grating:** $b2tol < 3*10^{-8} l/mm^3$ and $b3tol < 3*10^{-10} l/mm^4$. The looser tolerances can be accepted at the expense of reduced performance in the low energy operation range of both pre-mirrors.

The **tolerances on vls parameters in the case of a short (120 mm) grating** are much looser: $b2tol < 1*10^{-6} l/mm^3$ and $b3tol < 1*10^{-8} l/mm^4$. The tolerance on the *b2* parameter has been achieved in the production of provisional grating by Jobin-Yvon (see Sec. 3): $b2 = -1.2*10^{-6} l/mm^3$ ($b2 = -1.22*10^{-6} l/mm^3$) has been measured by Jobin-Yvon (European XFEL metrology [6]).

3 Performance of provisional short laminar grating compared to long blazed grating

The design grating for the soft X-ray monochromator in the SASE3 beamline is a 500 mm long blazed 50 l/mm grating with a blaze angle of 0.1°. Because of difficulties in the production of this grating, a provisional laminar 120 mm long 50 l/mm grating has been produced holographically by Jobin-Yvon.

The provisional grating has been characterized by Jobin-Yvon and XFEL metrology [6]. As discussed Section 2.2, the tolerance on *b2* vls parameter has been achieved.

The surface error of the substrate for the short grating was measured 199 nrad rms slope error and 2.8 nm peak-to-valley height error. Such a slope error, which is larger than the < 50 nrad specified for a nominal 500 mm long grating, can be accepted because it does not degrade much the resolution, which decreases with decrease of number of illuminated grooves (i.e. with a decrease of the length of the grating if the grating is over-illuminated).

In this section, the performance of provisional short laminar grating is presented in comparison with the performance of design long blazed grating. Overall, the main consequences of the usage of provisional short grating compared to design long grating onto the beamline performance are (i) losses in transmitted FEL beam intensity due to lower efficiency (laminar groove profile) and limited geometrical transmission, (ii) lower resolving power, and (iii) corresponding smaller pulse elongation by the grating (although shorter pulses are desired for many experiments, the product of temporal and energy resolution increases for cut beam compared to a transmitted > 4*σ Gaussian profile beam).

Note that, in addition to lower efficiency, a lower damage threshold for laminar gratings compared to blazed gratings could demand for additional attenuation of incidence beam intensity.

Since short grating reduces nominal resolving power of the monochromator operating in 1st diffraction order, the possibility of operation in higher diffraction orders of the grating is considered. One of the applications demanding for an increase in resolving power is the operation of the monochromator in spectrometer mode (the imaging crystal positioned in the exit slit plane is used to image dispersed beam spectral distribution); relatively high resolving power could be needed to resolve single spikes in SASE FEL spectrum to allow temporal pulse characterization and monochromator optimization. The performance of monochromator operated with short grating in 2nd diffraction order is presented as well.

3.1 Efficiency

The grating efficiency depending on the groove profile has been estimated using “Reflec” code [3], which is part of the “Ray” package [4] developed at BESSY. The comparison of efficiencies in the case of blazed and laminar gratings is presented in Fig. 6. The efficiency of grating with a laminar profile is lower by about a factor of two than the efficiency of blazed grating. With 0.65 valley-to-spacing ratio and 16 nm depth laminar grating profile, the best efficiency over the SASE3 operation range can be achieved. These values have been specified and achieved with accepted accuracy: a valley-to-spacing ratio of 0.66 and a groove depth of 17.3 nm (14.9 nm) have been measured by Jobin-Yvon (European XFEL metrology [6]).

The efficiency of laminar grating operated in 2nd diffraction order is presented in Fig. 6 as well. The efficiency is acceptable for the operation of the monochromator in spectrometer mode for most of the operation range of SASE3.

Losses of beam intensity due to the geometrical cut of the beam on grating are discussed in Sec. 3.2 and 3.6.

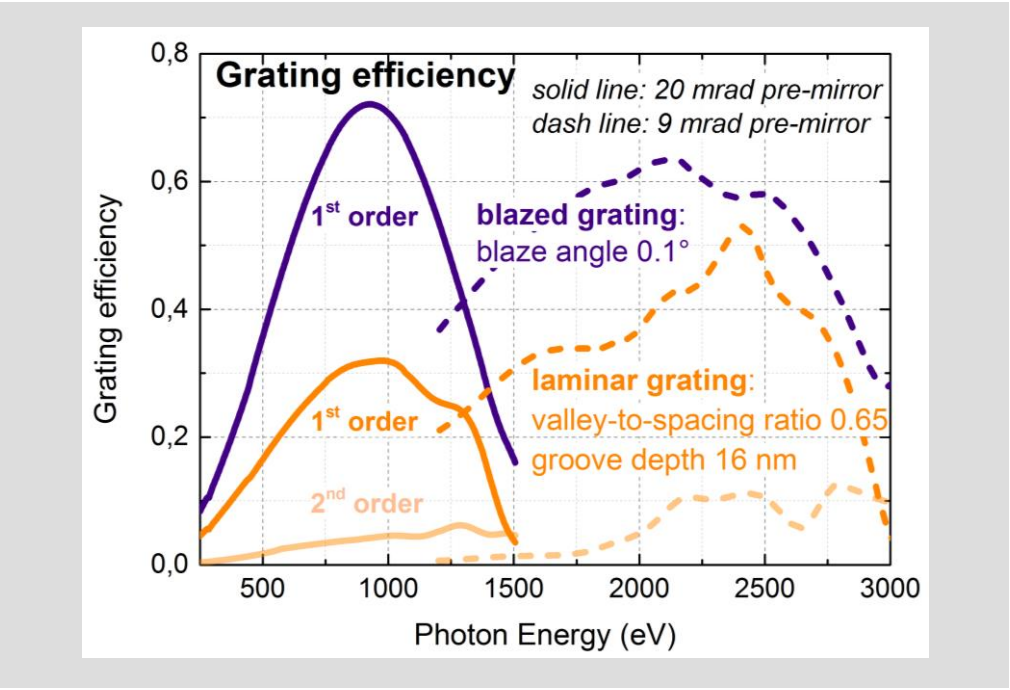

Figure 6: *Efficiency of 50 l/mm grating of the SASE3 monochromator operated in 1st and 2nd diffraction order - dependence on groove profile*

3.2 Grating geometrical transmission

In addition to efficiency losses due to the laminar profile of provisional grating, an additional source of losses in the case of provisional grating is reduced geometrical transmission. To estimate beam footprint on optics, namely grating, and the consequent geometrical cut, the beam divergence has been estimated according to Ref. [7] based on the expected SASE beam properties presented in Ref. [8] for the case of low, 20 pC, electron beam charge corresponding to the case of large divergence. The resulting geometrical transmission (in σ of a Gaussian-like FEL beam cross-section) is presented in Fig. 7. Note that divergence can vary slightly for a higher charge (smaller nominal divergence) or a special mode of operation as the tapering regime, for instance, resulting in slightly different geometrical transmission. However, the effect of varying divergence on the geometrical transmission can be considered to be minor compared to the effect of the grating length. One can see in Fig.7 that a 500 mm long nominal grating allows for high geometrical transmission reaching above 4 σ in the high energy range of each pre-mirror,

while the short provisional grating cuts the beam to below 2 σ in the complete range of operation. Note that the pulse length - bandwidth product increases for the cut profile: even being close to Fourier-limited transport, the product of FWHM time and FWHM energy resolution increases by about a factor of 2 from Gaussian to flat-top profile.

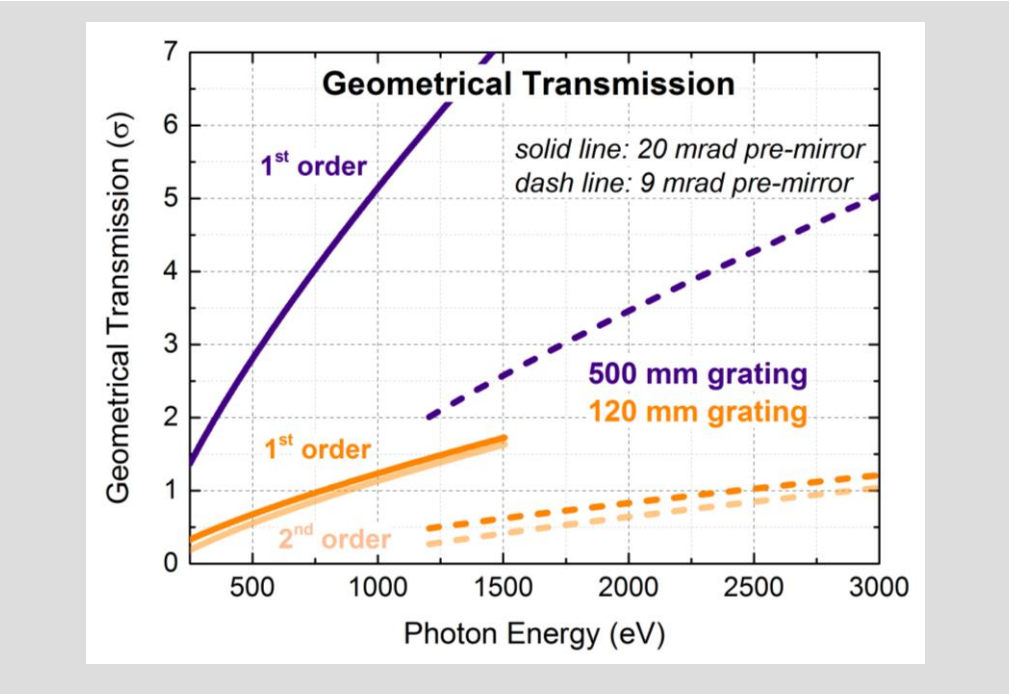

Figure 7: *Geometrical transmission (in σ of a Gaussian-like FEL beam cross-section) for the 500 mm long and 120 mm long 50 l/mm grating*

The overall transmission through the exit slit is presented and discussed in Sec. 3.6

3.3 Instrument response function

The instrument response function was estimated analytically using the Fourier transform of the spatial beam profile after the grating and combining the resulting function with an estimation of deterioration due to slope error on the optics surface. The results are presented in Fig. 8. The width of the instrument response function increases from about 20 µm (in the case of a nominal 500 mm long grating) to about 50 µm and above for the < 1 keV

spectral range for the case of short grating. The wavefront propagation simulation has been done to confirm the results of analytical estimations. The instrument response functions for provisional short and nominal long 50 l/mm gratings obtained using WPG framework for the case of 800 eV are presented in Fig. 9. The surface error of the short grating corresponds to the grating installed into the beamline. One can see good agreement between the analytical estimations and wavefront propagation simulations. The main effect seen in the shape of the instrument response function of the short grating is fringes due to cut of the beam on the grating aperture; the asymmetric effect of slope error seen in the case of a long grating is negligible in the case of a short one.

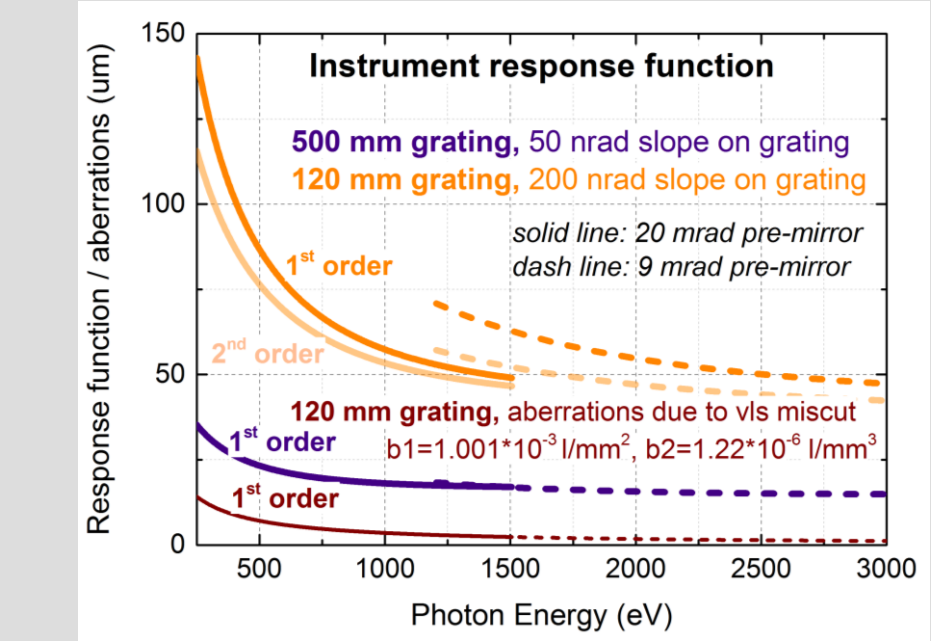

Figure 8: *Instrument response function in the focal plane for the 500 mm long (50 nrad rms slope error) and 120 mm long (200 nrad rms slope error) 50 l/mm grating*

In addition, aberrations due to the *b2* vls parameter miscut of the provisional grating produced by Jobin-Yvon have been estimated analytically as discussed in Sec. 2. As one can see in Fig. 8, these aberrations are well below the width of the instrument response function and can be neglected.

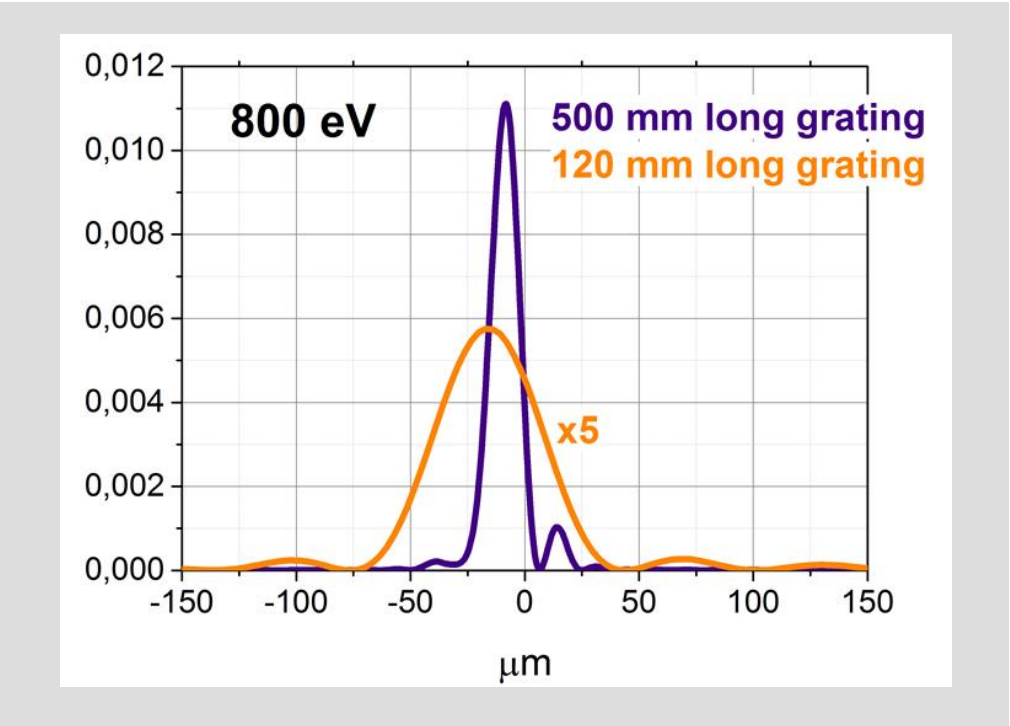

Figure 9: *Instrument response function in the focal plane for 800 eV photon energy in the case of a 500 mm long (40 nrad rms slope error and 3.4 nm peak-to-valley height error) and a 120 mm long (199 nrad rms slope error and 2.8 nm peak-to-valley height error) 50 l/mm grating calculated with the WPG framework*

3.4 Resolving power

Analytically estimated resolving power corresponding to the instrument response function discussed in the previous section is presented in Fig. 10. The resolving power is reduced from about 10000 ÷ 20000 expected in the case of a nominal 500 mm long grating down to about 5000 for the short provisional grating. The effect is mainly driven by a reduced number of illuminated grooves in the case of a short grating. To achieve a higher resolving power with the short grating, the operation in 2nd diffraction order can be considered (Fig. 10).

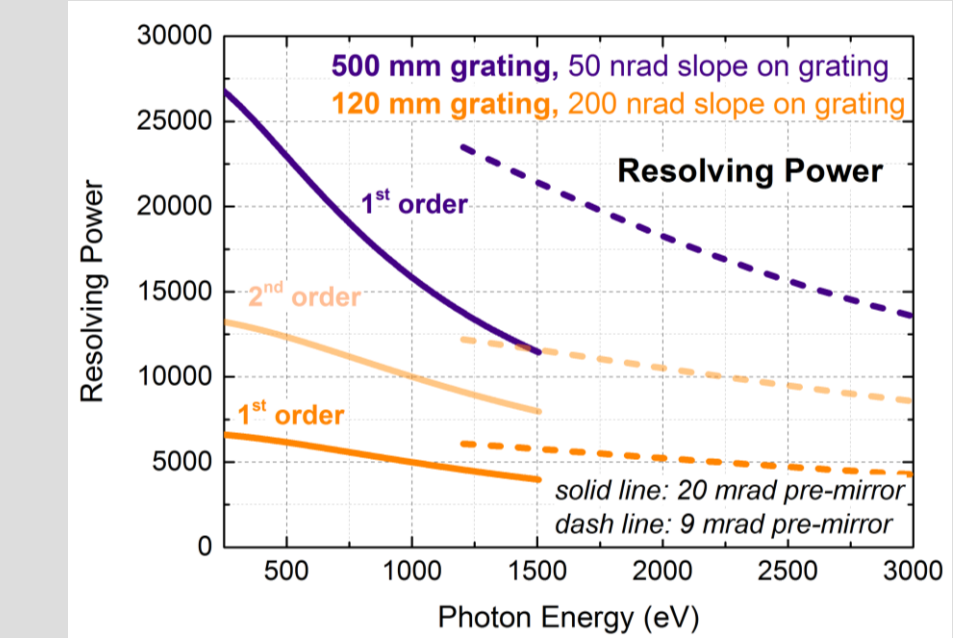

Figure 10: *Resolving power of the 500 mm long (50 nrad rms slope error) and 120 mm long (200 nrad rms slope error) 50 l/mm grating*

3.5 Temporal elongation

Along with the reduction of energy resolution due to the lower overall number of illuminated grooves in the case of the provisional 120 mm long grating, the pulse elongation becomes smaller (Fig. 11). The pulse stretching of the short grating operating in 1st diffraction order stays below 20 fs for the energies above 1250 eV and below 100 fs in the complete energy range of SASE3 beamline operation.

To reduce further the pulse stretching by the monochromator, the aperture before the monochromator can be used [9]. Expected pulse stretching versus aperture opening is shown in Fig. 12 for the cases of 290 eV, 500 eV, and 800 eV.

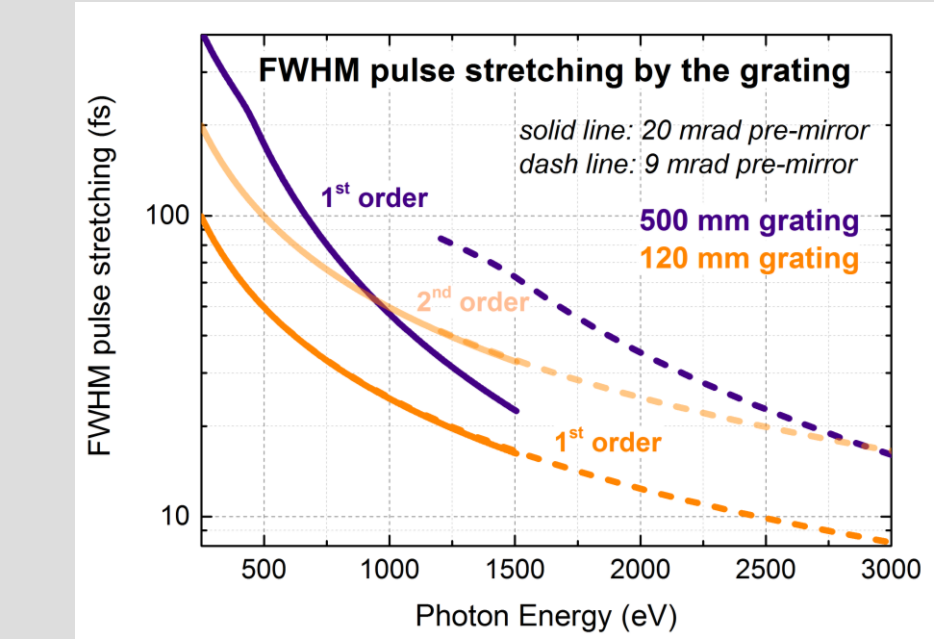

Figure 11: *FWHM pulse stretching by a 500 mm long and 120 mm long 50 l/mm grating*

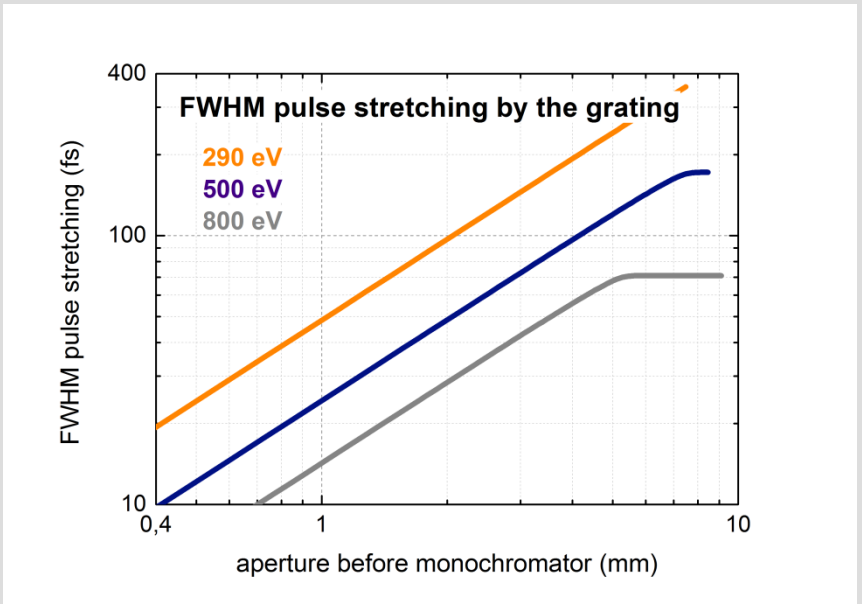

Figure 12: *FWHM pulse stretching by the monochromator operating in 1st order of a 50 l/mm grating depending on aperture width before the monochromator*

3.6 Transmission through exit slit

The transmission through the exit slit has been estimated analytically assuming 0.5% FEL bandwidth. The results are presented in Fig. 13. Transmission through a 20 µm slit (thick lines) is reduced by about one order of magnitude for the provisional short laminar (groove depth 16 nm) grating compared to nominal 500 mm long blazed (blaze angle 0.1°) grating. This reduction in transmission is due to (i) the reduced efficiency of laminar grating compared to blazed grating discussed in Sec. 3.1 and to (ii) the geometrical cut on the short grating discussed in Sec. 3.2. However, in the case of the short grating, the instrument response function in the focal plane corresponding to the best achievable energy resolution is larger than in the case of the 120 mm long grating (Sec. 3.3). So, in the case of 120 mm long grating, loss of flux due to the cut on the grating aperture can be compensated by opening the exit slit wider without a loss in resolution (if the focus size on the sample, which is an image of the exit slit, allows the exit slit to be opened wider). The transmission through the exit slit opened wider to the value of the instrument response function is shown in Fig. 13 as thin lines.

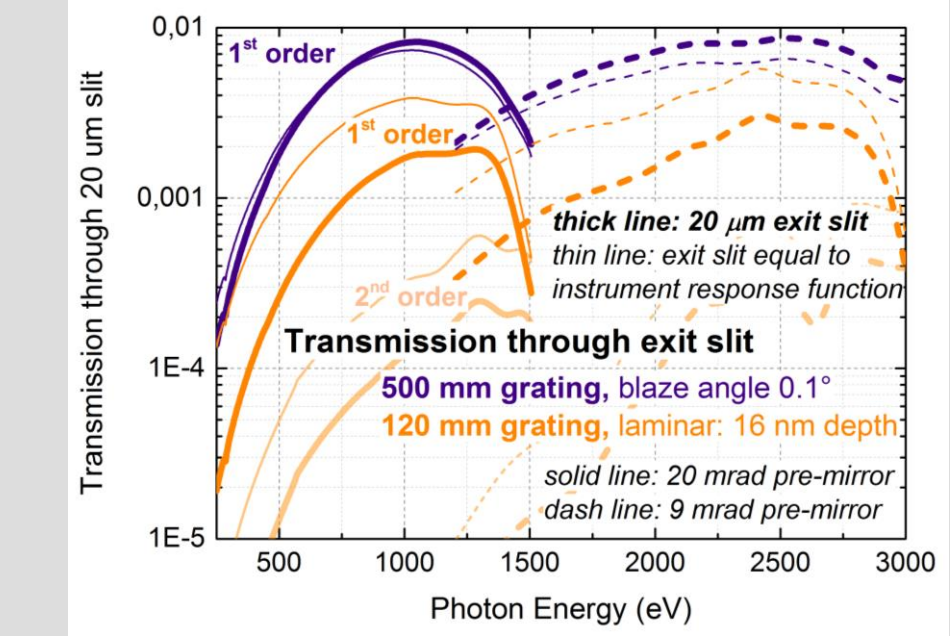

Figure 13: *Transmission through exit slit for the 500 mm long blazed (blaze angle 0.1°) and 120 mm long laminar (groove depth 16 nm) 50 l/mm grating. Thick lines: 20 µm exit slit. Thin lines: exit slit corresponding to the instrument response function.*

A References

[1] H. Sinn, M. Dommach, X. Dong, et al.: “Technical Design Report: X-Ray Optics and Beam Transport”, XFEL.EU TR-2012-006 (2012) doi:10.3204/XFEL.EU/TR-2012-006

[2] H. Noda, T. Namioka, M. Seya: “Geometric theory of the grating”, Journal of the Optical Society of America **64**, 1031 (1974) doi:10.1364/JOSA.64.001031

[3] F. Schäfers, M. Krumrey: “REFLEC - a program to calculate VUV and soft x-ray optical elements and synchrotron radiation beamlines”, BESSY Technischer Bericht TB 201, 1 (1996)

[4] F. Schäfers: “Ray - the BESSY raytrace program to calculate synchrotron radiation beamlines”, BESSY Technischer Bericht TB 202, 1 (1996)

[5] L. Samoylova, A. Buzmakov, O. Chubar, H. Sinn: “WavePropaGator: interactive framework for X-ray free-electron laser optics design and simulation”, Journal of Applied Crystallography **49**, 1347 (2016) doi:10.1107/S160057671600995X

[6] M. Vannoni, I. Freijo-Martin: “Absolute, high-accuracy characterization of a variable line spacing grating for the European XFEL soft X-ray monochromator”, Optics Express **25**, 26519 (2017) doi:10.1364/OE.25.026519

[7] H. Sinn, M. Gaudin, L.Samoylova, et al.: “Conceptual Design Report: X-Ray Optics and Beam Transport”, XFEL.EU TR-2011-002 (2011) doi:10.3204/XFEL.EU/TR-2011-003

[8] E. Schneidmiller, M.Yurkov: “Photon beam properties at the European XFEL”, TR-2011-006 (data files) (2011) doi:10.3204/DESY11-152

[9] A. Scherz et al.: “Conceptual Design Report: Scientific Instrument Spectroscopy and Coherent Scattering (SCS)”, XFEL.EU TR-2013-006 (2013) doi:10.3204/XFEL.EU/TR-2013-006

B Acknowledgements

The author is grateful to colleagues from the European XFEL X-Ray Optics group and the Scientific Instrument Spectroscopy and Coherent Scattering (SCS) group, in particular to Harald Sinn and Andreas Scherz for discussions about the SASE3 beamline design, performance, and expectations, and to Liubov Samoylova for guiding the work with the WPG framework.